energies

MDPI

Article

Deformation Study of Lean Methane-Air Premixed Spherically Expanding Flames under a Negative Direct Current Electric Field

Chao Li, Xiaomin Wu *, Yiming Li and Juncai Hou

Institute of Internal Combustion Engine, Xi'an Jiaotong University, Xi'an 710049, China; wzer1987@stu.xjtu.edu.cn (C.L.); liyimingl@stu.xjtu.edu.cn (Y.L.); houjuncai@stu.xjtu.edu.cn (J.H.)
* Correspondence: xmwu@mail.xjtu.edu.cn; Tel.: +86-29-8266-8721; Fax: +86-29-8266-8789

Academic Editor: Thomas E. Amidon
Received: 16 June 2016; Accepted: 7 September 2016; Published: 12 September 2016

Abstract: This paper compares numerical simulations with experiments to study the deformation of lean premixed spherically expanding flames under a negative direct current (DC) electric field. The experiments, including the flame deformation and the ionic distribution on the flame surface were investigated in a mesh to mesh electric field. Besides, a numerical model of adding an electric body force to the positive ions on the flame surface was also established to perform a relevant simulation. Results show that the spherical flame will acquire an elliptical shape with a marked flame stretch in the horizontal direction and a slight inhibition in the vertical direction under a negative DC electric field. Meanwhile, a non-uniform ionic distribution on the flame surface was also detected by the Langmuir probe. The simulation results from the numerical model show good agreement with experimental data. According to the velocity field analysis in simulation, it was found the particular motion of positive ions and neutral molecules on the flame surface should be responsible for the special flame deformation. When a negative DC electric field was applied, the majority of positive ions and colliding neutral molecules will form an ionic flow along the flame surface by a superposition of the electric field force and the aerodynamic drag. The ionic flow was not uniform and mainly formed on the upper and lower sides, so it will lead to a non-uniform ionic distribution along the flame surface. What's more, this ionic flow will also induce two vortexes both inside and outside of the flame surface due to viscosity effects. The external vortexes could produce an entraining effect on the premixed gas and take away the heat from the flame surface by forced convection, and then suppress the flame propagation in the vertical direction, while, the inner vortexes would scroll the burned zones and induce an inward flow at the horizontal center, which could be the reason for the pitted structure at the horizontal center when a high voltage was applied.

Keywords: lean combustion; electric field assisted combustion; ionic distribution; numerical simulation; spherically expanding flame

1. Introduction

As a potential assisted combustion technology, electric field assisted combustion has become of great interest in many combustion fields. Present techniques in this field are based on the application of direct current/alternating current (DC/AC) electrical potentials on various flames. Using these techniques, flames could be stabilized [1], propagation speed and burning velocity could be enhanced [2–4], and low soot formation can be achieved by using this technology in lean combustion techniques [5–7].

The classical explanation of how the DC electric field acts on a flame was the ionic wind effect [8–10], which refers to a result of the electric field force acting on the charged ions on the

flame surface. It had been proved that there were plenty of ions in the combustion, which led to the electrical properties of the flame surface. Once an electric field was applied, these ions would be driven by the electric field force and undergo a migration. The momentum of the charged ions would be transferred to other neutral molecules by collisions, and thus generating a bulk flow to promote the heat and mass transfer between the flame surface and premixed fuel which finally leads to the ionic wind effect.

Recent studies of the ionic wind effect had been conducted on many factors, such as the change of chemical reaction kinetics, ionic distribution of one-dimensional model and extra mass diffusion by the electric field in various types of flame, such as Bunsen flames [11–15], jet flames [16,17], flat flames [18–22], droplet flames [23], counter-flow flames [24,25], and spherically expanding flames [26,27]. Only a few studies have focused on the changes in the flow field caused by the electric effect. In fact, Hu et al. [9], Yamashita et al. [28] and Ulybyshev [29] had proved the electric field had an impact on the flow field, and even the ionic and molecular distribution, but this effect was not significant in the stagnant flame because the stagnant flame had an initial flow field, so the slight change of the flow field had a limited effect on it. What's more, these researches always concentrated on the new equilibrium state of the flame due to the fully developed of the ionic wind in the stagnant flame, so the ionic mass diffusion and the chemical reaction kinetics, which are related to the new ionic concentration distribution, would occupy a dominant position.

However, this conclusion may not be applicable in the transient flame, for example the premixed spherically expanding flame discussed in this paper, because this flame did not have an initial flow field. What's more, due to the continuous propagation of the flame surface and the short burning time, the new electric equilibrium state by the external electric field and the ionic distribution on the flame surface could not be reached at each moment. Therefore, the effect of the chemical reaction kinetics and the ionic mass diffusion based on the new ionic distribution, should be comparatively low in transient flames.

Additionally, some studies had found that spherically expanding flames could produce some special shapes under the negative DC electric field which were hard to explain by the conventional ionic wind theory. For instance, a pit on the flame surfaces in Meng's work [27]. A reasonable explanation for this phenomenon is also needed.

Based on these considerations, a simplified two-dimension (2-D) simulation model of a spherically expanding flame under a negative DC electric field was designed, and the simulation results were used to compare with the experimental results. By analyzing the flame shape, flame propagation speed, ionic distribution and the change in the flow field, the cause of the special deformation in the spherically expanding flame under negative DC electric field was explored.

2. Experimental Set up

2.1. Experimental Apparatus

There were two kinds of experimental apparatus, which were used to obtain the flame deformation and the ionic concentration respectively. The external systems for the two experiments were the same as what was used in the past [27,30,31], and consisted of six parts, including a constant-volume combustion chamber system, a fuel supply, an ignition control circle, an optical Schlieren system, a high-speed camera and a high-voltage supply system, as shown in Figure 1.

The combustion chamber, made of carbon steel, was a cylinder with an inner diameter of 130 mm and a length of 130 mm. An insulating bush made of polytetrafluoroethylene (PTFE) with an inner diameter of 115 mm, a thickness of 7.5 mm and a length of 130 mm was installed inside the combustion chamber. Two quartz windows with a 145 mm diameter were mounted on two sides of the chamber to allow optical accessibility. The ignition electrodes were located in the vertical direction along the chamber centerline and were surrounded by the PTFE to insulate the electrics, and will be grounded after the ignition. A high-speed digital camera (HG-100K, RedlakMothion Xtra, Beijing, China)

with a shooting speed of 5000 frames per second was used to take photos of the flames during the flame propagation.

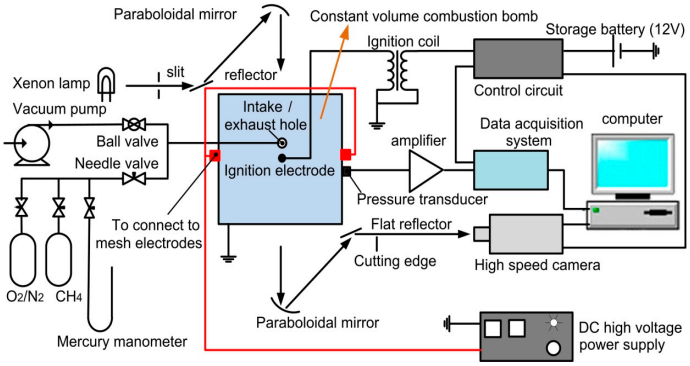

Figure 1. Schematic of the experimental setup.

Figure 2a shows the electrode arrangement for the flame deformation. Two high-voltage mesh electrodes with an outer diameter of 60 mm were installed horizontally and symmetrically 35 mm away from the ignition electrodes. The mesh electrodes were connected with a high-voltage DC power supply (DEL30N45, Wisman Company, Xianyang, China) with a voltage range from 0 kV to −5 kV to produce the electric fields between the ignition electrode and the mesh electrode.

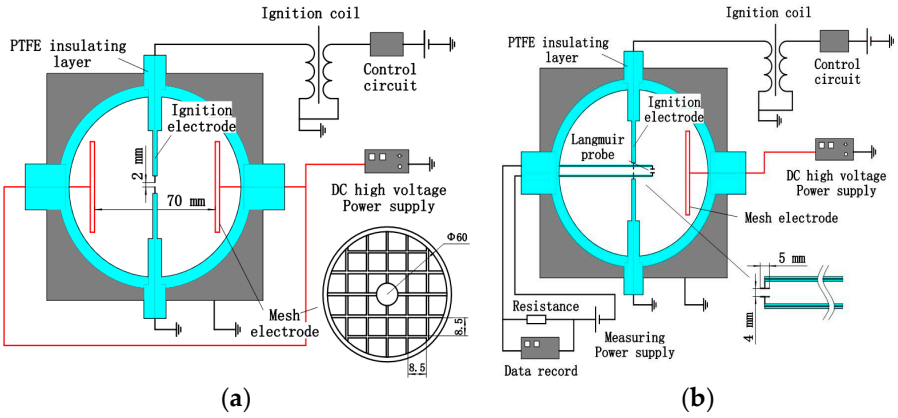

Figure 2. Electrode arrangement in the combustion chamber: (**a**) two mesh electrode type; and (**b**) one mesh electrode one Langmuir probe type.

Figure 2b shows the electrode arrangement for the ionic concentration experiments. A high-voltage mesh electrode was installed on the right side of the chamber to generate the electric field and a self-made Langmuir probe with a complete measuring circuit was installed on the left side to measure the ionic signal at the certain points required. The Langmuir probe, which was made of carbon steel, was a plate to plate type with a diameter of 4 mm and a spacing of 5 mm for the measuring head, and the rest part of the probe was covered with PTFE. The power supply for the Langmuir probe was 400 V, which was in the linear voltage-current region [32], and series resistance was 150 kΩ.

There were four certain points for the ionic concentration measurement in total, and their positions are shown in Figure 3. Among them, two measuring points were located at the horizontal centerline 10 mm and 20 mm away from the ignition source, which were defined as Points 1 and 2, respectively, while, the other two measuring points, defined as Points 3 and 4, respectively, were located at the side position 7 mm away from the horizontal centerline in the vertical direction, and 10 mm and 20 mm away from the ignition in the horizontal direction.

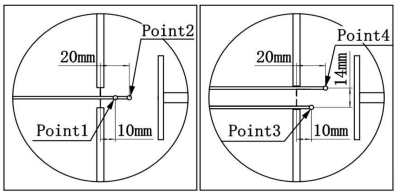

Figure 3. Position of the four measuring points.

2.2. Experimental Process

The combustible mixture was prepared by sequentially introducing CH_4 and O_2/N_2 synthesis gas (21% O_2 and 79% N_2 by volume) with the corresponding partial pressures, which were monitored by a U-tube mercury manometer. A time delay of 150 s was set to make sure the fuel and the oxidizer were perfectly mixed and there was no flow before ignition. The deformation of the flame was recorded by the high-speed camera system and the ionic concentration was noted by the Langmuir probe. Each experiment was repeated at least ten times under the same conditions to eliminate the errors.

3. Numerical Set up

3.1. Geometry

The numerical geometry is shown in Figure 4, which was based on the experimental apparatus geometry. To save on computational load, the numerical simulation was carried out on a 2-D Cartesian axisymmetric coordinate system. The domain region was a rectangle with 65 mm in the horizontal direction and 130 mm in the vertical direction. The up, down and right edges were all walls. The left edge was the symmetry axis, and two ignition electrodes were set close to the symmetry axis with the width of 1.5 mm and a length of 60 mm. The mesh electrodes were not included in the simulation model, as they had little effect on the flow field and only the experimental data before the flame reaches the mesh electrode was used.

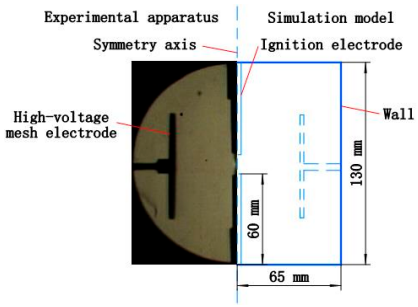

Figure 4. 2D computational domain compared with the experimental apparatus.

3.2. Numerical Assumption

To discuss how the negative DC electric field acts on the transient propagation flame, some reasonable assumptions are necessary. First, the change of ionic mass diffusion by the electric field was neglected in this model, and it should be noted that this assumption was only applicable for the transient flame, for example, the spherically expanding flame described in this paper. This assumption was made because the transient propagation flame could not provide a sufficient time (at least 10 ms according to Marcum [13] and Kim [15]) for the ions and electrons on the flame surface to reach a new electrical equilibrium or develop well at each moment, as in a stagnant flame. Han's simulations [33], which refer to the negative applied voltage that had little effect on the ionic and electronic concentration on the flame premixed side in a one dimension (1-D) freely propagating premixed flame, also support this view. Based on this reason, it was possible that the dominant ionic distribution should still depend

on the motion of the flow field in the spherically expanding flame, and the extra ionic mass diffusion, which relate to the possible new ionic and electric equilibrium state, should be very small, and could be neglected in a spherically expanding flame.

Second, this paper only focused on the positive ionic wind effect, so the effects of negative ions and electrons were neglected. In DC electric field assisted combustion, the negative ions are always neglected because the concentration of negative ions is very low, about 2 orders of magnitude lower than that of the positive ions [34,35], and they are mainly formed in later stages of combustion. Meanwhile, the impact of electrons in this model is also small, because the applied voltages on the mesh electrodes are negative in this paper, so the direction of the electric field was from the ignition electrodes to the mesh electrodes (to the right in the simulation part of Figure 4). For this reason, only positive ions were driven to the premixed zone to produce the ionic wind effect, while electrons would be removed to the burned zone rapidly, due to their low number density and extremely high mobility (K = 4000 $cm^2/s/V$) [36], which is at least three orders of magnitude higher than that of ions (K = 1.0 $cm^2/s/V$) [28,37]. Although some research had shown that electrons may produce the excitation of nitrogen and other molecules by collisions [19,20], however, these chemical activation steps ocurred in the burned zones in this paper, so they would not have an obvious effect on the outward flame propagation.

3.3. Governing Equations

This model was an unsteady propagating flame model which was coupled with a complex chemical reaction mechanism and an extra electric body force. The governing equations were the Navier-Stokes (N-S) hydrodynamic equations including the conservation of mass (1), momentum (2) and energy (3):

$$\frac{\partial \rho}{\partial t} + \mathbf{div}(\rho \mathbf{u}) = 0 \tag{1}$$

$$\frac{\partial (\rho u)}{\partial t} + \mathbf{div}(\rho \mathbf{u} u) = \mathbf{div}(\rho v \mathbf{grad} u) - \mathbf{grad} p + \mathbf{S}_e \tag{2}$$

$$\frac{\partial (\rho H)}{\partial t} + \mathbf{div}(\rho \mathbf{u} H) = \mathbf{div}(\lambda \mathbf{grad} T) + \frac{\partial p}{\partial t} + \mathbf{u} \cdot \mathbf{grad} p + \Phi + Q + \mathrm{S}_H \tag{3}$$

where, $\mathbf{S}_e$ is electrical body force. S_H is the heat release by the electric effect.

The electrical body force $\mathbf{S}_e$ is shown in Equation (4) based on the definition of the Coulomb force:

$$\mathbf{S}_e = \mathbf{E} q c_t \tag{4}$$

where, q was the unit charge of ions. c_i was the positive ionic concentration. The electric field intensity $\mathbf{E}$ is defined as the gradient of the electric potential U in Equation (5):

$$\mathbf{E} = -\alpha_u \mathbf{grad} U \tag{5}$$

where, a_u was the uniform coefficient. Previous studies [30,31,38] have verified that our electrode arrangement could only produce an approximately uniform electric field between the ignition and the mesh electrode, and a_u was about 0.7 in the main study zone for −2.5 kV and −5 kV electric field.

3.4. Reaction Mechanism

The fuel in this paper was a $CH_4/O_2/N_2$ mixture, so the reduced GRI 3.0 neutral mechanism proposed by Smooke [39] including the 19-species and 70-reactions were selected as the main reaction mechanism. Besides, a reduced ionic reaction mechanism [33,40], which was described in Table 1 by six reactions, including CHO^+ and H_3O^+ that account for more than 95% of the total positive ions in lean combustion, was also added into the mechanism as a supplement. As this paper mainly focuses on the change of the flow field, but not the change of ionic reaction, the reduced ionic reaction mechanism should be acceptable in our simulation.

Table 1. Adopted ionic reactions.

Reaction Type	Elementary Reaction	(A, n, E_a) *
Chemi-Ionization	$CH + O \rightarrow HCO^+ + e^-$	2.51×10^{11}, 0.0, 1700
Proton transfer	$HCO^+ + H_2O \rightarrow H_3O^+ + CO$	1.51×10^{15}, 0.0, 0.0
Recombination	$H_3O^+ + e^- \rightarrow H_2O + H$	2.29×10^{18}, 0.5, 0.0
	$H_3O^+ + e^- \rightarrow OH + H + H$	17.95×10^{21}, 1.4, 0.0
	$H_3O^+ + e^- \rightarrow H_2 + OH$	1.25×10^{19}, 0.5, 0.0
	$H_3O^+ + e^- \rightarrow O + H_2 + H$	6.00×10^{17}, 0.3, 0.0

* Reaction rate: $k = AT^n \exp(-E_a/RT)$. Units: cm, mol, cal, K, s.

3.5. Boundary Conditions

All simulations were carried out using the commercial software FLUENT. The mesh type in this model was actriangle with the maximum size of no more than 0.1 mm. The ignition zone was located at the left center of the domain, it was a semi-circle with a radius of 1 mm. The other zones were the premixed zones. The premixed gas was a $CH_4/O_2/N_2$ mixture with an excess air coefficient of 1.6. The initial temperature in premixed zones was 300 K, and the initial pressure was 101,325 Pa. The ignition was started by patching 3000 K to the ignition zone. All the walls in this model were set to 300 K based on the property parameters of PTFE, which was the same as the experiments, to calculate the heat release.

4. Result and Discuss

4.1. Flame Shape and Propagation Speed

Figure 5 shows the comparison of the flame shape between the simulation and the experiment under applied voltages of 0, −2.5 and −5 kV. The flame shapes in the simulation and experiments were given by the temperature contour lines and Schlieren images, respectively.

From Figure 5a, it could be found that the flame shapes in the simulation and experiments all showed a smooth circle in the absence of applied voltage. Even though there was a heat release on the ignition electrode, this effect was obviously not strong enough to inhibit flame propagation in the vertical direction, so the flame still showed an approximately circular shape with a temperature of 2080 K in the burned zones. When the applied voltage increases to −2.5 kV, the flame will become an ellipsoidal shape with a promotion in the horizontal direction and an inhibition in the vertical direction, as shown in Figure 5b. Besides, the curvature radius of the flame surface was also changed due to the different flame propagation speeds in different directions. When the applied voltage increased to −5 kV, the flame still showed that the horizontal propagation was stretched and the vertical propagation was suppressed. However, a pit like structure was found being formed at the horizontal center of the flame surface, and this structure appeared in both the simulation and experiments.

For a better analysis of the deformation process, Figure 6 shows the result of the flame propagation speed change with time in the horizontal center and vertical center directions in the simulation and experiments, under the voltages of 0, −2.5 and −5 kV, respectively. The propagation speed in the two directions was defined as $v_h = \mathrm{d}r_h/\mathrm{d}t$ and $v_v = \mathrm{d}r_v/\mathrm{d}t$, where r_h and r_v were the flame radius along the horizontal centerline and the vertical centerline.

In Figure 6a, it could be found that in the absence of electric field, the flame propagation speed was basically uniform. The flame propagation speed in the horizontal direction was about 0.56 m/s, and the propagation speed in the vertical direction was slightly lower, at about 0.53 m/s. This phenomenon should be ascribed to the influence of the ignition electrode, which causes a drag and extra heat release to the flame, so that the vertical flame propagation was weakly affected. The simulation results were scaled in this figure, so that the propagation speed matched. The scaling factor was defined as the

flame propagation speed ratio between experiment and simulation under 0 kV, and this scaling factor would be used in the comparison under the electric field of −2.5 kV and −5 kV.

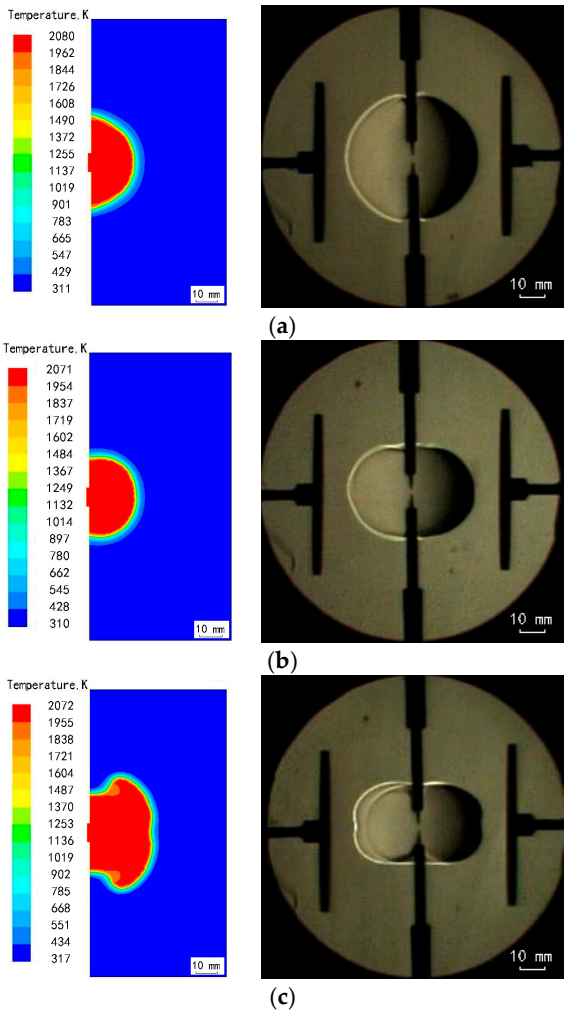

Figure 5. Flame shape in simulation and experimental Schlieren images: (**a**) 0 kV, 45 ms; (**b**) −2.5 kV, 38 ms; and (**c**) −5 kV, 34 ms.

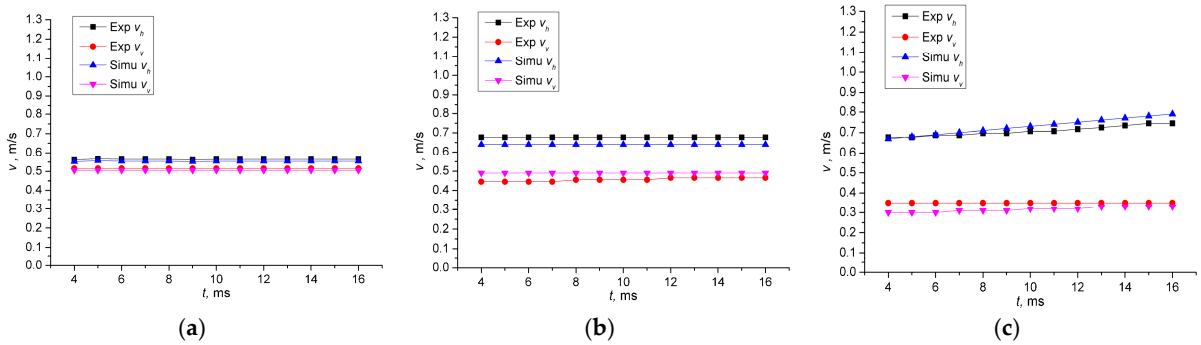

Figure 6. Flame propagation speed in the two directions in simulation and experiment: (**a**) 0 kV; (**b**) −2.5 kV; and (**c**) −5 kV.

Figure 6b is the result under −2.5 kV. The flame propagation speed in the two directions was still approximately uniform. In the experiment, the horizontal flame propagation speed had increased to 0.68 m/s, which was 0.12 m/s higher than that under 0 kV, while the vertical flame propagation

speed was reduced to 0.46 m/s, which was 0.04 m/s lower that under 0 kV. The simulation results showed the same tendency, but a less large change compared with the experiment. The horizontal flame propagation speed increased to 0.64 m/s, and the vertical flame propagation speed is reduced to 0.48 m/s. The average relative errors of the simulation compared with the experiment were about 5.7% and 4.6% in the horizontal and vertical directions, and the peak relative errors were 5.8% and 6.4%, which occur at 10 ms and 4 ms, respectively.

Figure 6c is the result under −5 kV. The flame propagation speed in the horizontal direction in the experiment had increased to 0.7 m/s, which was 0.02 m/s higher than that under −2.5 kV at 4 ms. Besides, the propagation speed also showed an extra tendency to gradually accelerate from 4 ms to 16 ms, and the flame propagation speed at 16 ms had reached to 0.75 m/s. The vertical propagation speed continued to decrease to 0.35 m/s, which was 0.14 m/s lower than under −2.5 kV. The propagation speed change in simulation also showed the same tendency as the experiment. The horizontal flame propagation increased to 0.7 m/s at 4 ms and accelerated to 0.79 m/s at 16 ms, while, the vertical flame propagation speed was reduced to 0.3 m/s. The average relative errors between the simulation and the experiment were 1.8% and 6.4% in the horizontal and vertical directions, and the peak relative errors were 3.6% and 9.6%, which occur at 16 ms and 4 ms, respectively.

In general, it was clear that the simulation results were in good agreement with the experiments. This similarity was not only reflected in the flame shape, including the flame promotion in the horizontal direction, the flame inhibition in the vertical direction and the pit structure on the flame surface, but also in the curvature radius change of the flame surface, and even the flame propagation speed in different directions. This could prove that the simulation method could provide a good prediction for the spherically expanding flame under a negative DC electric field.

4.2. Explanation of Flame Deformation

To explain the special flame shape, including the flame stretch in the horizontal direction, the flame inhibition in the vertical direction and the pit at the horizontal center, the velocity vectors and the local figure, which showed the ionic and molecular motion law, were extracted, as shown in Figure 7.

In Figure 7a, it could be found that the flow field will maintain its original propagation rate without an electric field. Ions and neutral molecules on the flame surface only had a slight outward diffusion due to the temperature difference between the burned zone and premixed zone. Special ionic motion, such as the extra ionic flows and vortexes, were not found in this case.

In Figure 7b,c, it could be found that when the electric field was applied, several special ionic motions will be formed in the flow field. First, the direction of the electric field was defined pointing to the right horizontally, so the positive ions on the flame surface must have a tendency to accelerate and escape from the flame surface to the premixed zones (purple mark in Figure 7), just like the conventional ionic wind effect. However, due to the insufficient response time, it was hard for this ionic wind effect to fully develop in the propagating flame, so only a small part of the positive ions on the flame surface respond to the electric field force [13,15], and then collide with the other neutral molecules on the flame surface. This effect could also promote the heat and mass transfer between the reaction zone and the premixed region by further ionic and molecular collisions, and then promote the flame propagation speed in this direction. This should the main reason for the flame propagation promotion in the horizontal direction.

Second, additional bulk ionic flows along the flame surface were formed (red mark in Figure 7). This kind of ionic flow was produced by the superposition effect of both the electric field force and the aerodynamic drag on the remaining positive ions. Among them, the electric field force on the positive ions was always to the right, according to the electrode arrangement and the applied voltages, while, the aerodynamic drag [41], which was produced by the reverse ionic and molecular concentration gradient and the electric potential gradient by the already moved ions, would be only formed at the boundary between the premixed zone and the reaction zone due to the different motion states (reaction zone was driven, premixed zone was almost static). The aerodynamic drag would prevent the

remaining positive ions and other neutral molecules from further motion to the premixed region, but not hinder the ions and molecules from moving along the flame surface, so under the combined action of the two forces, the remaining positive ions and colliding molecules would produce an ionic flow along the flame surface. This ionic flow was mainly formed at the upper and lower sides of the flame surface, because there was a certain angle between the electric field force and the aerodynamic drag at these positions. This angle will gradually increase from the vertical center (90°) to the horizontal center (180°), so the resultant force on the positive ions would also gradually decrease from the vertical center to the horizontal center. For this season, the velocity of the ionic flow along the flame surface may also gradually decrease from the vertical center to the horizontal center, and then produce a non-uniform ionic flow along the flame surface. This ionic flow seldom reached the horizontal center, which should be primarily ascribed to the fact that the aerodynamic drag and electric field force took an opposite direction (180°) at the horizontal center.

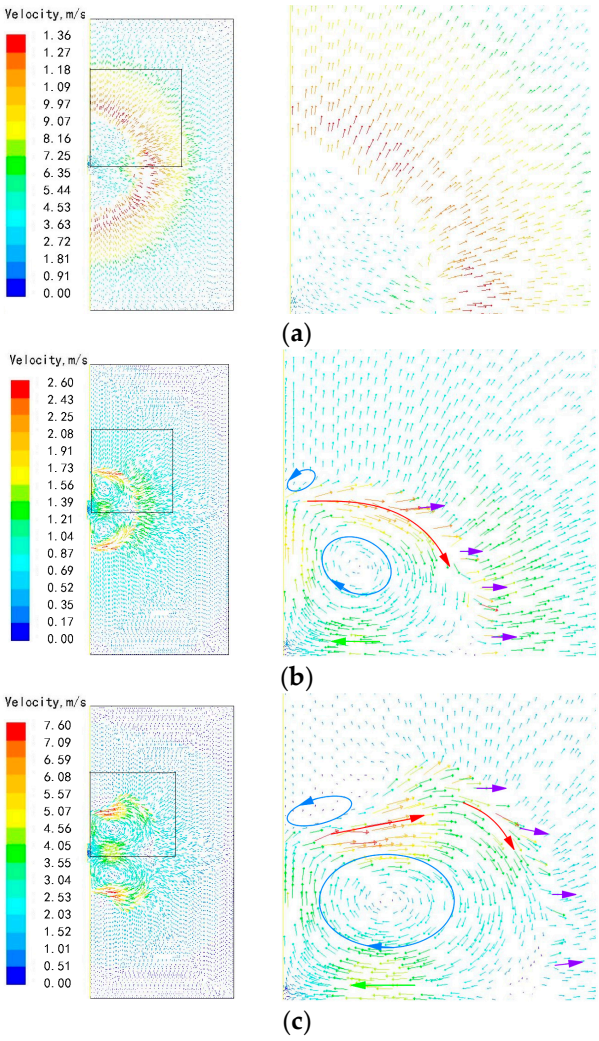

Figure 7. Velocity vector in simulation: (**a**) 0 kV; (**b**) −2.5 kV; and (**c**) −5 kV.

Third, two vortexes (blue mark in Figure 7) were also found both inside and outside of the flame surface when the electric field was applied. This phenomenon should be due to the effect of gas viscosity. When the ionic flow along the flame surface was formed (red mark in Figure 7), the molecules on both sides of the ionic flow would also be driven due to the gas viscosity. As the flow field must be continuous, the gas on both sides of the ionic flow need to form vortexes. The external vortexes were mainly formed in the vertical center, and it would drive the premixed gas into the

flame surface and take away the heat from the flame surface by the entrainment effect [42], so that a visible flame propagation inhibition could be obtained in the vertical center, while, the inner vortexes were symmetrical in the burned zone, and it will promote the heat transfer between the burned zones and the reaction zones [42], so the temperature in the burned zones showed a slightly lower value in Figure 5 when the electric field was applied. The inner vortexes will also induce an inward ionic flow in the burned zones at the horizontal center (green mark in Figure 7), and drag the flame surface causing further propagation at the center position. This should be the reason for the pit on the flame surface at the horizontal center.

Finally, the intensity of all kinds of ionic and molecular motion, including the various ionic flows (purple, red and green mark in Figure 7) and the vortexes (blue mark in Figure 7), all increased with the increase of the applied voltage. For example, the average velocity of the ionic flow along the flame surface was about 2.43 m/s under −2.5 kV, while it reached to 7.09 m/s when the electric potential was −5 kV. For this reason, the flame deformation induced by the flow field, such as flame stretching in the horizontal direction, the flame inhibition in the vertical direction and the overall flame change will all increase with the increase of the applied voltage. This should be the reason why the flame shape modification becomes more pronounced with the increase of the applied voltage.

4.3. Ionic Concentration Distribution

The velocity field in simulations had shown that there were ionic flows being formed along the flame surface with the electric field. The ionic flow was not uniform, and it was mainly formed at the upper and lower sides of the flame surface, but seldom affected the horizontal center. As it was hard to measure the ionic flow in the closed chamber directly, the change of ionic concentration, which was a result of the unequal ionic flow, was measured experimentally to verify the simulation.

Figure 8 is the direct voltage data from the Langmuir probe. To simplify, the data under 0, −2.5 and −5 kV at the four measuring points were selected for introduction.

In Figure 8, it can be seen that the ionic signal will be obtained only when the flame surface reaches the Langmuir probe, because the major ions were mainly formed on the flame surface. The power supply for the Langmuir probe was a constant, so the ionic signal could directly reflect the ionic concentration at the measuring point, and the peak value of the ionic signal represents the peak ionic concentration [31]. Figure 8a,b shows that when the electric field was not loaded, the peak value of the ionic signal at the center and the side position (Points 1–4) were all near 0.3 V, which means the ionic concentration distribution was almost uniform on the flame surface without the electric field.

However, Figure 8c,d shows that when a −2.5 kV voltage was applied, the peak ionic signal at the center positions (Points 1 and 2) reduced to 0.2 V, and the peak ionic signal at the side positions (Points 3 and 4) increased to 0.7 V. In Figure 8e,f, this changing tendency of the ionic signal will continue, the peak ionic signal at the center positions (Points 1 and 2) reduced to 0.11 V, and the peak ionic signal at the side positions (Points 3 and 4) increased to 0.79 V.

Figure 8 clearly reflected that when a negative voltage was applied, the ionic concentration along the flame surface will be changed from a uniform distribution to a non-uniform distribution. At the center position, the ionic signal gradually decreased with the increase of the applied voltage, while, at the side position, the ionic signal gradually increased with the increase of the applied voltage. Figure 9 is the line chart of the peak ionic signal at the four fixed measuring points under a negative electric field from 0 kV to −5 kV in 0.5 kV increments.

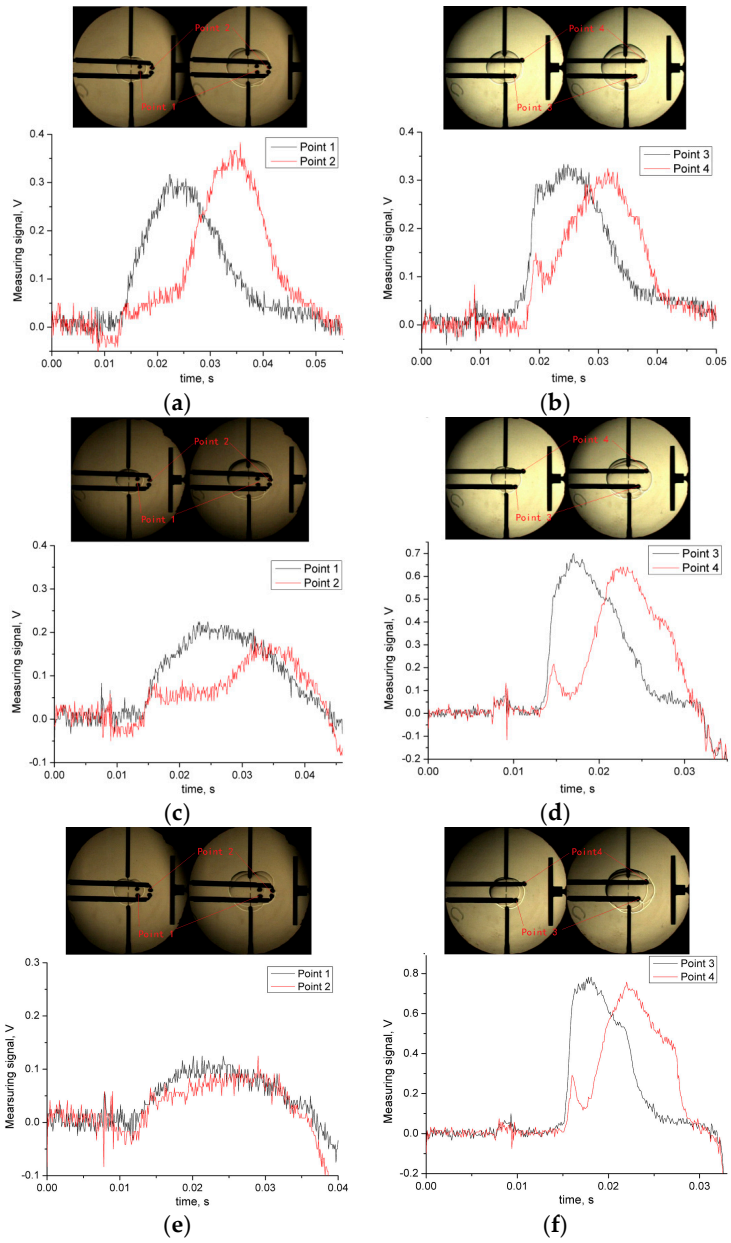

Figure 8. Ionic signal with flame position: (**a**) 0 kV center; (**b**) 0 kV side; (**c**) −2.5 kV center; (**d**) −2.5 kV side; (**e**) −5 kV center; and (**f**) −5 kV side.

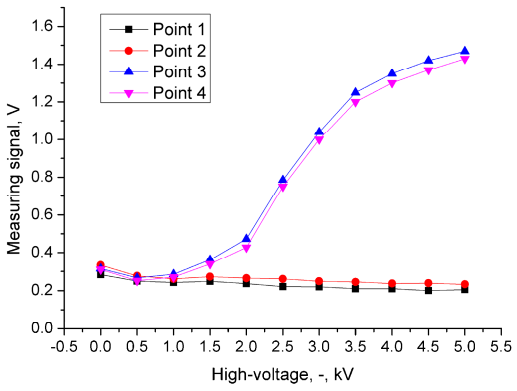

Figure 9. Peak ionic concentration change at the four points under various voltages.

The peak ionic signal had been modified in this figure because the electric field by the voltage on the mesh electrode may reduce the effective section area of the Langmuir probe, and the modified factor of the ionic signal could be calculated by Equation (6), where, U was the applied voltage on mesh electrode:

$$\alpha_s = 1/\sin(\arccos 0.176U) \quad (6)$$

In Figure 9, it could be found that the peak ionic signals were basically the same with the value of 0.3 V at the four fixed points at the beginning, which means the ionic concentration distribution on the flame surface should be uniform when the applied voltage was 0 kV. However, when the electric field was applied, the peak ionic signal showed a significant difference between the center (Points 1 and 2) and the side (Points 3 and 4) positions.

At the center position, the peak ionic signal at Point 1 only underwent a slight decrease from 0.28 V to 0.21 V and the peak ionic signal at Point 2 decreased from 0.33 V to 0.24 V with the increase of the applied voltage on the mesh electrode, while, the peak ionic signal showed a significant increase from 0.32 V to 1.47 V at Point 3 and from 0.31 V to 1.43 V at Point 4, respectively, with the increase of the applied voltage.

This phenomenon can be explained by the simulation result of the ionic flow along the flame surface (red mark in Figure 7). At the center position, the ionic flow along the flame surface seldom reached this region, so the slight decrease of the peak ionic signal should be due to the outward migration of some ions by the electric field. At the side position, the peak ionic signal will be affected by two factors. On the one hand, the outward migration of ions from the peak signal position will slightly reduce the peak ionic signal, which was the same as that at the center position. On the other hand, due to the presence of ionic flow at the side position, the peak ionic signal will also be affected by the influx and outflux of the positive ions in this region. In the simulation part, it had been found that the velocity of the ionic flow along the flame surface gradually decreased along its flow direction (the vertical center was the maximum, the horizontal center was close to 0, and the side position was somewhere in between), that is to say, the outflux of the ions at each point at the side position should be smaller than the influx of the ions. For this reason, there must be an increase in the ionic concentration at the side position, which leads to an increase of the peak ionic signal, just as what was measured in the experiment. The phenomenon whereby the peak ionic signal gradually increased with the applied voltage should be due to that the increase of the applied voltage may elevate the velocity gradient of the ionic flow, and then improve the accumulation rate of the positive ions.

5. Conclusions

In this paper, the deformation process of the spherically expanding flame under a negative DC electric field was studied by both experiments and numerical simulation. By analyzing the flame shape, the ionic concentration distribution in the experiment and flow field in the simulation, the main conclusions can be summarized as follows:

(1) The simulation method of adding an extra electric body force to the positive ions could make a good prediction for the negative DC electric field acting on the spherically expanding flame, including the flame shape, flame propagation speed and some special flame structure.

(2) When a negative DC electric field was applied on a spherically expanding flame, a small part of the ions and other neutral molecules on the flame surface would be driven to the premixed zone by the electric field, and then promote the flame propagation in the electric field direction. Besides, the majority of ions and neutral molecules will form an ionic flow moving along the flame surface. This kind of ionic flow was usually formed on the upper and lower sides of the flame surface by the superposition effect of the electric field force and the aerodynamic drag, and it will lead to a non-uniform ionic concentration distribution on the flame surface.

(3) The ionic flow along the flame surface would induce two vortexes both inside and outside of the flame surface due to the viscosity. The outside vortex would obviously inhibit the flame

propagation in the vertical direction by entraining the premixed gas into the flame surface and take away the heat from the flame surface, while, the inside vortex would induce a secondary inward flow and then change the flame shape, even forming a pit structure at the center position.

Acknowledgments: The authors gratefully acknowledge the National Natural Science Foundation of China (Grant No. 51476126).

Author Contributions: Chao Li carried out all the experiments, simulation and wrote the manuscript. Xiaomin Wu designed all the experiments and revised the manuscript. Yiming Li and Juncai Hou helped Chao Li finished the experiment and also gave some suggestions.

Conflicts of Interest: The authors declare no conflict of interest.

Nomenclature

E	electrical field intensity
H	static enthalpy
K	mobility
c_i	concentration of ions
p	pressure
Q	heat release
S	source term
t	time
T	temperature
q	element charge
u	horizontal velocity
v	vertical velocity
Φ	viscous dissipative term
λ	thermal conductivity
ν	dynamic viscosity
ρ	density
r_h, r_v	flame radius in horizontal and vertical direction
v_h, v_v	flame propagation speed in horizontal and vertical direction
a_u	uniform coefficient of the electric field
a_s	modified factor of effective section area of the Langmuir probe

References

1. Kim, W.; Do, H.; Mungal, M.G.; Cappelli, M.A. Optimal discharge placement in plasma-assisted combustion of a methane jet in cross flow. *Combust. Flame* **2008**, *153*, 603–615. [CrossRef]
2. Ombrello, T.; Won, S.H.; Ju, Y. Flame propagation enhancement by plasma excitation of oxygen. Part I: Effects of O_3. *Combust. Flame* **2010**, *157*, 1906–1915.
3. Ombrello, T.; Won, S.H.; Ju, Y. Flame propagation enhancement by plasma excitation of oxygen. Part II: Effects of $O_2(a1\Delta g)$. *Combust. Flame* **2010**, *157*, 1916–1928. [CrossRef]
4. Tao, R.; Huang, K.; Tang, H.; Bell, D. Electrorheology leads to efficient combustion. *Energy Fuels* **2008**, *22*, 3785–3788. [CrossRef]
5. Cha, M.S.; Lee, S.M.; Kim, K.T.; Chung, S.H. Soot suppression by nonthermal plasma in coflow jet diffusion flames using a dielectric barrier discharge. *Combust. Flame* **2005**, *141*, 438–447. [CrossRef]
6. Vega, E.V.; Shin, S.S.; Lee, K.Y. NO emission of oxygen-enriched $CH_4/O_2/N_2$ premixed flames under electric field. *Fuel* **2007**, *86*, 512–519. [CrossRef]
7. Zhang, Y.; Wu, Y.; Yang, H. Effect of high-frequency alternating electric fields on the behavior and nitricoxide emission of laminar non-premixed flames. *Fuel* **2013**, *109*, 350–355. [CrossRef]

8. Altendorfner, F.; Kuhl, J.; Zigan, L. Study of the influence of electric fields on flames using planar LIF and PIV techniques. *Proc. Combust. Inst.* **2011**, *33*, 3195–3201. [CrossRef]
9. Hu, J.; Rivin, B.; Sher, E. The effect of an electric field on the shape of co-flowing and candle-type methane–air flames. *Exp. Therm. Fluid Sci.* **2000**, *21*, 124–133. [CrossRef]
10. Vega, E.V.; Lee, K.Y. An experimental study on laminar $CH_4/O_2/N_2$ premixed flames under an electric field. *J. Mech. Sci. Technol.* **2008**, *22*, 312–319. [CrossRef]
11. Wisman, D.L.; Marcum, S.D.; Ganguly, B.N. Electrical control of the thermo diffusive instability in premixed propane-air flames. *Combust. Flame* **2007**, *151*, 639–648. [CrossRef]
12. Ata, A.; Cowart, J.S.; Vranos, A.; Cetegen, B.M. Effects of direct current electric field on the blow off characteristics of bluff-body stabilized conical premixed flames. *Combust. Sci. Technol.* **2005**, *177*, 1291–1304. [CrossRef]
13. Marcum, S.D.; Ganguly, B.N. Electric-field-induced flame speed modification. *Combust. Flame* **2005**, *143*, 27–36. [CrossRef]
14. Sakhrieh, A.; Lins, G.; Dinkelacker, F.; Hammer, T.; Leipertz, A.; Branston, D.W. The influence of pressure on the control of premixed turbulent flames using an electric field. *Combust. Flame* **2005**, *143*, 313–322. [CrossRef]
15. Kim, M.K.; Chung, H.S.; Kim, H.H. Effect of electric fields on the stabilization of premixed laminar Bunsen flames at low AC frequency: Bi-ionic wind effect. *Combust. Flame* **2012**, *159*, 1151–1159. [CrossRef]
16. Lee, S.M.; Park, C.S.; Cha, M.S.; Chung, S.H. Effect of electric fields on the liftoff of non-premixed turbulent jet flames. *IEEE Trans. Plasma Sci.* **2005**, *33*, 1703–1709.
17. Borgatelli, F.; Dunn-Rankin, D. Behavior of a small diffusion flame as an electrically active component in a high-voltage circuit. *Combust. Flame* **2012**, *159*, 210–220. [CrossRef]
18. Volkov, E.N.; Sepman, A.V.; Kornilov, V.N.; Konnov, A.A.; Shoshin, Y.S.; de Coey, L.P.H. Towards the mechanism of DC electric field effect on flat premixed flame. In Proceedings of the European Combustion Meeting, Vienna, Austria, 14–17 April 2009.
19. Vandenboom, J.; Konnov, A.; Verhasselt, A.; Kornilov, V.; Degoey, L.; Nijmeijer, H. The effect of a DC electric field on the laminar burning velocity of premixed methane/air flames. *Proc. Combust. Inst.* **2009**, *32*, 1237–1244. [CrossRef]
20. Sanchez-Sanz, M.; Murphy, D.C.; Fernandez-Pello, C. Effect of an external electric field on the propagation velocity of premixed flames. *Proc. Combust. Inst.* **2015**, *35*, 3463–3470. [CrossRef]
21. Stockman, E.S.; Zaidi, S.H.; Miles, R.B.; Carter, C.D.; Ryan, M.D. Measurements of combustion properties in a microwave enhanced flame. *Combust. Flame* **2009**, *156*, 1453–1461. [CrossRef]
22. Prager, J.; Riedel, U.; Warnatz, J. Modeling ion chemistry and charged species diffusion in lean methane–oxygen flames. *Proc. Combust. Inst.* **2007**, *31*, 1129–1137. [CrossRef]
23. Patyal, A.; Kyritsis, D.; Matalon, M. Electric field effects in the presence of chemi-ionization on droplet burning. *Combust. Flame* **2016**, *164*, 99–110. [CrossRef]
24. Dayal, S.K.; Pandya, T.P. Structure of counterflow diffustion flame in transverse electric fields. *Combust. Flame* **1979**, *35*, 277–287. [CrossRef]
25. Xie, L.; Kishi, T.; Kono, M. The influence of electric fields on soot formation and flame structure of diffusion flames. *J. Therm. Sci.* **1993**, *2*, 288–293. [CrossRef]
26. Cha, M.S.; Lee, Y. Premixed combustion under electric field in a constant volume chamber. *IEEE Trans. Plasma Sci.* **2012**, *40*, 3131–3138. [CrossRef]
27. Meng, X.W.; Wu, X.M.; Kang, C.; Tang, A.D.; Gao, Z.Q. Effects of direct-current (DC) electric fields on flame propagation and combustion characteristics of premixed $CH_4/O_2/N_2$ flames. *Energy Fuels* **2012**, *26*, 6612–6620.
28. Yamashita, K.; Karnani, S.; Dunn-Rankin, D. Numerical prediction of ion current from a small methane jet flame. *Combust. Flame* **2009**, *156*, 1227–1233. [CrossRef]
29. Ulybyshev, K.E. Calculation of the effect of a constant electric field on the gas dynamics and nitrogen oxide emission in laminar diffusion flame. *Fluid Dyn.* **2000**, *35*, 38–42. [CrossRef]
30. Duan, H.; Wu, X.M.; Zhang, C.; Cui, Y.C.; Hou, J.C.; Li, C.; Gao, Z.Q. Experimental study of lean premixed $CH_4/N_2/O_2$ flames under high frequency alternating-current electric fields. *Energy Fuels* **2015**, *29*, 7601–7611. [CrossRef]

31. Duan, H.; Wu, X.M.; Sun, T.Q.; Liu, B.; Fang, J.F.; Li, C.; Gao, Z.Q. Effects of electric field intensity and distribution on flame propagation speed of $CH_4/O_2/N_2$ flames. *Fuel* **2015**, *158*, 807–815. [CrossRef]
32. Jacobs, S.V.; Xu, K.G. Examination of ionic wind and cathode sheath effects in a E-field premixed flame with ion density measurements. *Phys. Plasmas* **2016**, *23*. [CrossRef]
33. Han, J.; Casey, T.; Belhi, M.; Arias, P.G.; Bisetti, F.; Im, H.G.; Chen, J.Y. Modeling of the effect of an electric field on the distribution of charged species in 1D premixed flames. In Proceedings of the 10th Asia-Pacific Conference on Combustion, Beijing, China, 19–22 July 2015.
34. Goodings, J.M.; Bohme, D.K.; Ng, C.W. Detailed ion chemistry in methane oxygen flames. I. Positive ions. *Combust. Flame* **1979**, *36*, 27–43. [CrossRef]
35. Goodings, J.M.; Bohme, D.K.; Ng, C.W. Detailed ion chemistry in methane oxygen flames. II. Negative ions. *Combust. Flame* **1979**, *36*, 45–62. [CrossRef]
36. Bisetti, F.; Morsli, M.E. Calculation and analysis of the mobility and diffusion coefficient of thermal electrons in methane/air premixed flames. *Combust. Flame* **2012**, *159*, 3518–3521. [CrossRef]
37. Fialkov, A.B. Investigations on ions in flames. *Prog. Energy Combust. Sci.* **1997**, *23*, 399–528. [CrossRef]
38. Fang, J.F.; Wu, X.M.; Duan, H.; Li, C.; Gao, Z.Q. Effects of electric fields on the combustion characteristics of lean burn methane-air mixtures. *Energies* **2015**, *8*, 2587–2605. [CrossRef]
39. Smooke, M.D.; Bilger, R.W. *Reduced Kinetic Mechanisms and Asymptotic Approximations for Methane-Air Flames*; Springer-Verlag: Berlin/Heidelberg, Germany, 1991; Volume 384.
40. Kim, D.; Rizzi, F.; Cheng, K.W.; Han, J.; Bisetti, F.; Knio, O.M. Uncertainty quantification of ion chemistry in lean and stoichiometric homogenous mixtures of methane, oxygen, and argon. *Combust. Flame* **2015**, *162*, 2904–2915. [CrossRef]
41. Pozrikidis, C. *Fluid Dynamics: Theory, Computation, and Numerical Simulation*, 2nd ed.; Springer Science Business Media: New York, NY, USA, 2009.
42. Lau, E.V.; Lee, J.R.; Mohamed Ismail, H. Forced convective heat transfer of ionic wind on different surface conditions. *Appl. Mech. Mater.* **2015**, *793*, 445–449.